Turbidity-based Aerial Perspective Rendering for Mixed Reality

CARLOS MORALES[†1] HONGXUN ZHAO[†1] REI KAWAKAMI[†2]
TAKESHI OISHI[†1] KATSUSHI IKEUCHI[†1]

Abstract: Achieving realistic results is one of the most important goals in outdoor Mixed Reality (MR) applications that are built by merging virtual objects into real scenes. One kind of these applications consists on viewing a virtual object that is distant from the observer. The objective in such applications is to realistically represent the atmospheric effect over the appearance of the virtual object. This natural effect over objects in open air scenes is known as aerial perspective and causes the color of distant objects to become fainter and shift towards the environmental light color. However, aerial perspective modeling is challenging since outdoor illumination is unpredictable and continually changing. In computer vision (CV) and computer graphics (CG), light scattering phenomena causing the aerial perspective effect are generally modeled by a combination of a directly transmitted light and an airlight. Using such model, several studies have been carried out for aerial perspective rendering in complete-virtual applications, but only Zhao [4] have presented a research applied to MR. His approach employs a straightforward adaption of Preetham's CG-directed aerial perspective model [2]; however, his implementation is a computer-intensive task. In this paper, we propose an improved scattering model for MR applications that is based on both a full visible spectrum of light analysis and an atmospheric turbidity estimation. Our method first estimates the atmospheric turbidity by matching the brightness distributions of a captured omnidirectional image and sky models. Then the estimated turbidity is utilized to render the aerial perspective effect as a summation of the direct transmission and the airlight.

Keywords: Mixed reality, rendering, aerial perspective, turbidity

1. Introduction

In outdoor Mixed Reality (MR) that consists on integrating virtual objects into real scenes, one of the main goals is to create real-time applications where the appearance of the inserted virtual object corresponds to the real scene's look. In real open-air scenes, when a target object viewed by an observer is far, the perceived object's appearance changes losing contrast and becoming blurred, as shown in Fig. 1. This natural effect is known as *aerial perspective* and is due to the light scattered by particles suspended in the atmosphere. Therefore, in outdoor MR applications where the target virtual object is distant from the observer, we need to render an artificial aerial perspective over the virtual object to emulate the natural atmospheric effect. However, handling with the changing and unpredictable natural atmospheric phenomena such as the environmental illumination and weather conditions, while implementing a fast rendering algorithm, is a challenging issue.

Common methods for aerial perspective modeling rely on understanding the scattering phenomena in the atmosphere. Such models vary depending on whether the aim is oriented to computer vision (CV) or computer graphics (CG). Representative works in outdoor scattering modeling include [1], [2], [3], [4]. McCartney [1] presented an excellent review of former works on atmospheric optics. His work, which has been widely used in CV and CG applications, contains relevant data about the scattering phenomena under different weather conditions categorized by the heuristic parameter *turbidity*. Preetham et al. [2] proposed a full-spectrum turbidity-based analytical sky model for various atmospheric conditions. Based on this model, they developed an approximated scattering model for aerial perspective representation in complete-virtual applications. Narasimhan and Nayar [3] proposed a

Figure 1. Natural aerial perspective effect over Tokyo. Appearance of distant mountains fades and blends with the horizon's color.

physics-based scattering model to describe the appearances of real scenes under uniform bad weather conditions. Surprisingly little work has been done on scattering modeling for MR. Recently, Zhao [4] proposed an RGB-based aerial perspective model for MR. He estimated the spectral sensitivities of various cameras and used these functions to go from spectral radiance to RGB pixel values. His method employs the spectral sensitivity of a camera used for capturing a real scene and uses a simple modification of the Preetham's scattering model to generate the aerial perspective effect over virtual objects inserted in the real scene. However, since he only used a straightforward adjustment of Preetham's model, the appearance of the synthesized virtual object suffers from a weak aerial perspective effect even for high turbidity values and large distances.

Aerial perspective modeling for MR essentially depends on how similar the synthesized aerial perspective effect and the natural one are. A conventional principle of solving such problem would be finding a scattering model with parameters that lead to generate a realistic synthesized appearance alike the real scene. For this purpose, we propose a full-spectrum turbidity-based aerial perspective model. Our approach benefits from two main contributions. The first is the robust and fast

---

†1 The University of Tokyo
†2 Osaka University

turbidity-estimation method. Our second contribution is our improved scattering model that uses a full-spectrum analysis, shows realistic results, and enables a fast rendering.

This paper is divided into eight sections. After introducing the background in Sect. 2, we present our proposed method for turbidity estimation in Sect. 3. Afterwards, our improved scattering model for MR is explained in Sect. 4. In Sect. 5, we provide the rendering equation to model the aerial perspective effect. The evaluation of our aerial perspective model and the experimental results are shown in Sect. 6 and 7 respectively. The last section completes this paper with discussion and conclusion.

2. Background

2.1 Atmospheric scattering

Propagation of environmental light through the atmosphere is governed by the scattering phenomena. Figure 2 illustrates a collimated beam of light with radiance $L(W \cdot sr^{-1} \cdot m^{-3})$ traveling a distance s trough a scattering medium. This beam will lose part of itself due to scattering out of the transmission path x, and the remaining light is modeled by

$$L(s,\lambda) = L_0(\lambda)e^{-t_{sc}(s,\lambda)} , \qquad (1)$$

where L_0 is the radiance at $x=0$ and t_{sc} is the optical thickness of the atmospheric path. The optical thickness conveys the combined total scattering effects of all the particles along the path x, and its value is expressed by

$$t_{sc}(s,\lambda) = \int_0^s \beta_{sc}(x,\lambda)dx , \qquad (2)$$

where β_{sc} is called the scattering coefficient.

The scattering coefficient depends on size of particles in the atmosphere, wavelengths, and directions of incident light. In the past, Rayleigh [5] and Mie [6] studied the atmospheric scattering caused by small and larger particles respectively.

2.1.1 Rayleigh scattering

Lord Rayleigh [5] studied the scattering of electromagnetic waves by particles, such as air molecules, much smaller than the wavelength "λ" of the electromagnetic wave. At height h from sea level, Rayleigh's scattering coefficient is given by

$$\beta_R = \frac{8\pi^3(n^2-1)^2}{3N\lambda^4}\left(\frac{6+3p_n}{6-7p_n}\right) \times e^{\frac{-h}{H_0}} , \qquad (3)$$

where $n=1.0003$ is the refractive index of air in the visible
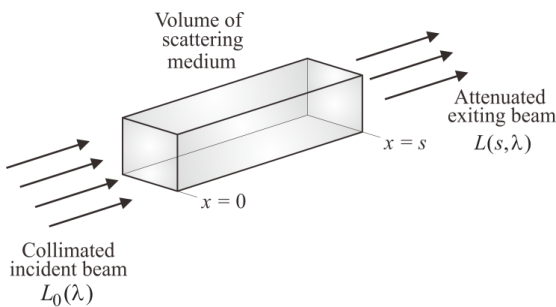

Figure 2. Atmospheric scattering of a collimated beam of light

spectrum, $p_n=0.035$ is the depolarization factor for air, $H_0=7994m$ is the scale height for small particles, and $N=2.545\times10^{25}m^{-3}$ is the molecular number density of the standard atmosphere.

2.1.2 Mie scattering

Mie [6] studied the scattering by particles whose size is nearly equal to the wavelength of the electromagnetic wave. In atmospheric optics, we can use Mie scattering for particles such as aerosol, water droplet, water drop, and so on. At height h from sea level, Mie's scattering coefficient is given by

$$\beta_M = 0.434c(T)\pi\left(\frac{2\pi}{\lambda}\right)^{v-2} K(\lambda) \times e^{\frac{-h}{H_0}} , \qquad (4)$$

where c is the concentration factor that depends on the atmospheric turbidity, $v=4$ is the Junge's exponent, K is the wavelength-dependent Fudge factor, and $H_0=1200m$ is the scale height for larger particles.

2.2 Atmospheric condition via turbidity

Atmospheric turbidity T is used to express a quantitative and straightforward characterization of atmospheric conditions. Using turbidity, we can identify atmospheric conditions such a clear day for $T=3$, a slightly hazy day for $T=7$, a significantly hazy day for $T=15$, and fog conditions for T above 20.

Turbidity is defined as the ratio of the optical thickness of the atmosphere composed by molecules of air (t_R) plus larger particles (t_M) to the optical thickness of air molecules alone [1]:

$$T = \frac{t_R + t_M}{t_R} , \qquad (5)$$

where t_R and t_M are calculated using Eq. (2), (3) and (4) for the Rayleigh and Mie scattering coefficients respectively.

2.2.1 The Preetham sky model

Preetham *et al.* [2] presented an analytical sky model for various atmospheric conditions through turbidity. Their model relates the luminance Y (cd/m²) of sky in any viewing direction V with respect to the luminance at a reference point Y_z by

$$Y = \frac{F(\theta, \gamma, T)}{F(0, \theta_s, T)}Y_z , \qquad (6)$$

where F is sky luminance distribution model of Perez *et al.* [7], θ is the zenith angle of viewing direction, θ_s is the zenith angle of the sun, and γ is the angle of the sun direction with respect to the viewing direction (see coordinates in Fig. 3).
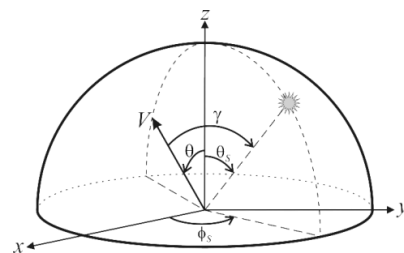

Figure 3. Coordinates in sky hemisphere. Observer is in the origin.

2.3 Aerial perspective model

The following optical model is widely used in dealing with outdoor scenarios under various weather conditions [3], [8], [9]:

$$L(s,\lambda) = L(0,\lambda)e^{-\beta_{sc}(\lambda)s} + L(\infty,\lambda)(1-e^{-\beta_{sc}(\lambda)s}) . \quad (7)$$

$L(s,\lambda)$ is the total light perceived by the observer. The first term is called *direct transmission* and refers to the light from the target that is not scattered as it travels through the viewing path until reaching the observer (see Fig. 4). The second term is the *airlight*, which stands for the environmental illumination that is scattered into the direct transmission path and then is attenuated in the way to the observer. $L(0,\lambda)$ is the light at the target, $L(\infty,\lambda)$ is the atmospheric light, $\beta_{sc}=\beta_R+\beta_M$ is the total scattering coefficient, and s is the distance between the target and the observer.

2.4 Rendering equation

In MR applications, we need an equation to go from the radiometric formulas such as the spectral radiance to pixel color values such as RGB. In general, when an object is illuminated by a source of light, the reflected light goes through the camera lens and is recorded by its charged couple device (CCD). Then the recorded image intensity for the channel $c \in \{r,g,b\}$ is obtained as

$$I_c = \int_{380\text{nm}}^{780\text{nm}} L(\lambda)q_c(\lambda)d\lambda , \quad (8)$$

where $L(\lambda)$ is the reflected spectral radiance at the object surface, 380 to 780nm stands for the visible spectrum of light, and $q_c(\lambda)$ is the spectral sensitivity of the camera.

The camera's spectral sensitivity is important for color correction of the virtual object since it compensates the effects of the recording illumination. In this matter, Zhao [4] used a turbidity-based method to calculate the spectral sensitivity of several cameras, so we will benefit from his data. .

3. Atmospheric turbidity estimation

An important goal in this research is provide a fast and robust approach for turbidity estimation that can handle a real-time implementation and can operate under different sky conditions including cloudy skies. We estimate turbidity by matching the brightness distribution of a captured omnidirectional image and the brightness distribution of Preetham's sky models. For this purpose, we minimize the following error function:

$$Err = \sum_{i=1}^{N} \left| \frac{Y_i(T)}{Y_{ref}(T)} - \frac{Y_i}{Y_{ref}} \right| , \quad (9)$$

where N is the number of sample points used in the calculation process, *ref* is the reference point that can be the zenith or any other point in the visible sky portion, $Y_i(T)/Y_{ref}(T)$ is the luminance ratio in the sky model, which can be obtained from Eq. (6), and Y_i/Y_{ref} is the luminance ratio in the captured
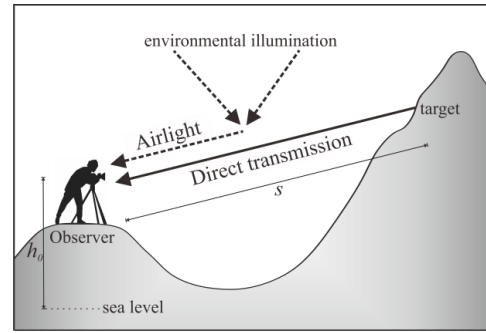

Figure 4. Aerial perspective modeled as summation of direct transmission and airlight.

image's pixel for Y channel of the XYZ color system. To solve Eq. (9), we use the Levenberg-Marquardt algorithm (LMA).

Our turbidity estimation approach uses a similar idea as in Zhao's work [4], however, differs in four aspects. First, we use random sampling points instead of uniform distributed patches in the sky. The second difference is that we use the Y channel from XYZ system for analyzing the luminance in the captured image instead of the total intensity of a pixel given by the summation of the intensities of *r*, *g*, and *b* channels. Third, we employ LMA for the error minimization instead of the Particle Swarm Optimization. The last difference is that our proposed method does not depend either on the camera or the white balance parameters. These differences provide a more flexible and robust approach, thus improving Zhao's results.

Since the Preetham sky model does not provide equations for calculating the brightness of cloudy pixels, the Random Sample Consensus (RANSAC) approach will be used in case of a cloudy sky. Basically, the RANSAC method arbitrarily chooses a fraction of the N sampling points as assumed inliers and estimates the turbidity using them. If the estimated turbidity is too high, there is a great probability that most of the inliers are cloudy pixels, thus we use the estimated turbidity to test the other sampling points. Here we calculate the *Err* corresponding to one sampling point, and if this is smaller than the threshold, we put it into the hypothetical inlier set. Then the turbidity value is estimated from the new inlier set, and we calculate *Err*. This procedure is repeated until the maximum iteration. Turbidity is estimated from the inlier set which has the smallest *Err*.

4. An improved scattering model for MR

Scattering models for MR requires parameters that guarantee a realistic result when implementing the aerial perspective effect over virtual objects. The scattering parameters used in Zhao's work [4] make a weak aerial perspective effect over virtual objects, thus making their appearances to blur and fade slightly, even at long distances from the observer and high turbidity values. To solve this problem, we propose an improved scattering model for MR applications based on McCartney's data [1]. We employ data in [1] about weather conditions through scattering coefficients, which is summarized in the
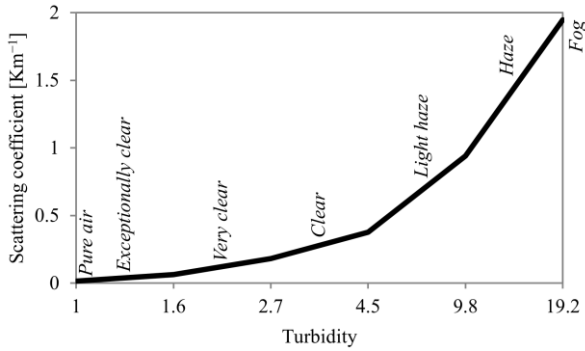
Figure 5. Scattering coefficients through turbidity and weather conditions.

Appendix, to provide a classification of scattering coefficients through turbidity, as illustrated in Fig. 5.

4.1 Rayleigh's scattering coefficient correction

We can obtain the value of the Rayleigh scattering coefficient of β_R=0.0141Km^{-1} for a spectrally weighted average wavelength (550 nm) from Table 3 in Appendix. However, using Eq. (3) for λ=550nm and h = 0m (standard conditions), we obtain β_R = 0.0135 Km^{-1}. Therefore, we propose a straightforward multiplicative correction factor K_R given by

$$K_R = \frac{0.0141}{0.0135} = 1.0396. \qquad (10)$$

Then our modified Rayleigh scattering coefficient is given by

$$\beta_R = \frac{8\pi^3(n^2-1)^2}{3N\lambda^4}\left(\frac{6+3p_n}{6-7p_n}\right)K_R \times e^{\frac{-h_0}{H_0}}, \qquad (11)$$

where n, p_n, H_0, and N are same as in Eq. (3), h_0 is the height at the observer, and K_R is given by Eq. (10).

4.2 Mie's scattering coefficient correction

One issue in Preetham's scattering model [2] is related to the turbidity itself. From the definition of turbidity in Eq. (5), T=1 refers to the ideal case where Mie's scattering coefficient is cero. This means that the concentration factor c in Eq. (4), which depends on the turbidity value, should be cero for T=1. Preetham used c=(0.6544T-0.6510)×10^{-16} and Zhao used a corrected c=(0.6544T-0.6510)×10^{-18} for MR. However, by simple inspection we can deduce that this factor is not cero for T=1. Hence, we propose a concentration factor given by

$$c(T) = (0.65T - 0.65)\cdot 10^{-16}. \qquad (12)$$

Another important issue is the value of the Fudge factor K used by Preetham and Zhao. They used a wavelength-dependent K whose value varies between 0.65 and 0.69 for wavelengths ranging from 380–780nm. In fact, we can deduce this Fudge factor from [1]. Preetham considered a turbidity of 1.6 for an exceptionally clear weather condition. From Table 4, an exceptionally clear condition is categorized by a Mie scattering coefficient of 0.0639Km^{-1}. Thus, we can solve Eq. (4) under standard conditions (λ=550nm and h=0m) and calculate a corrected and Fudge factor under such conditions. The obtained

Fudge factor after following this procedure was estimated as

$$K_M = 0.0092. \qquad (13)$$

Note that Preetham's Fudge factor [2] is almost 70 times our proposed Fudge factor. This is the main reason why the direct transmission in Preetham's aerial perspective model varies so drastically in relation to the turbidity and distance, thus resulting in an abrupt changing of objects' appearances even for low turbidity values and short distances from the observer. Besides, another important difference with Preetham's Fudge factor is that our factor does not depend on wavelength. Then our modified Mie scattering coefficient can be written as

$$\beta_M = 0.434c(T)\pi\left(\frac{2\pi}{\lambda}\right)^{v-2}K_M \times e^{\frac{-h_0}{H_0}}, \qquad (14)$$

where c is given by Eq. (12), K_M is given by Eq. (13), and υ, h_0, and H_0 are same as in Eq. (4).

5. Aerial perspective rendering

The aerial perspective rendering equation is obtained by replacing the aerial perspective model (direct transmission and airlight of Fig. 4) of Eq. (7) in the rendering equation of Eq. (8). From these equations, the observer perceives the intensity value I_c of a virtual object's pixel at distance s for the channel c$\in$\{r,g,b\} as

$$I_c(s) = \int_{380\text{nm}}^{780\text{nm}} L(0,\lambda)e^{-\beta_{sc}(\lambda,T,h_0)s}q_c(\lambda)d\lambda +$$
$$\int_{380\text{nm}}^{780\text{nm}} L(\infty,\lambda)(1-e^{-\beta_{sc}(\lambda,T,h_0)s})q_c(\lambda)d\lambda \qquad (15)$$

where $L(0,\lambda)$, $L(\infty,\lambda)$, and s are same as in Eq. (7); and h_0 and β_{sc}=β_R+β_M are same as in Eq. (11) and (14).

In daylight applications, it is common to assume that $L(\infty,\lambda)$ is globally constant, thus obtaining its value from pixels in the sky near the horizon that have the highest intensity value. Besides, we do not have the value of $L(0,\lambda)$ since the target object is a CG model. To solve this problem, we can approximate the spectral sensitivity in the direct transmission and airlight of Eq. (15) by a Dirac's delta function. Therefore, we propose the following aerial perspective rendering equation:

$$I_c(s) = I_{0,c}\cdot\Gamma_c(s) + I_{\infty,c}(1-\Gamma_c(s)), \qquad (16)$$

where $I_{0,c}$ is the intensity value of a pixel at the surface of the virtual object, $I_{\infty,c}$ is the highest intensity value of a pixel at an infinite distance in the input image, and Γ_c is the attenuation factor calculated as

$$\Gamma_c(s) = \frac{\int_{380\text{nm}}^{780\text{nm}}e^{-\beta_{sc}(\lambda,T,h_0)s}q_c(\lambda)d\lambda}{\int_{380\text{nm}}^{780\text{nm}}q_c(\lambda)d\lambda}, \qquad (17)$$
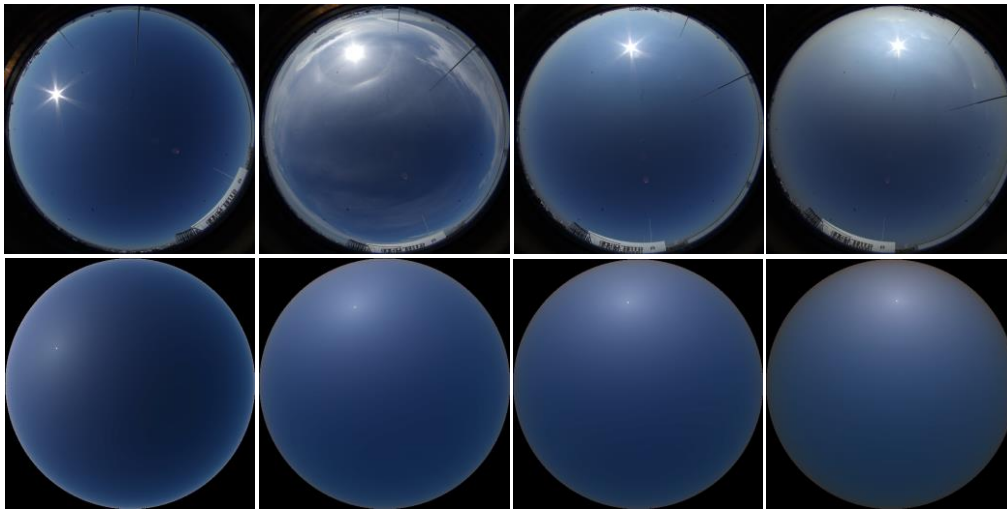
Figure 6. Turbidity estimation results. (Top) Pictures by Canon EOS5D with fisheye lens. Estimated turbidities from left to right: T=1.9, T=2.52, T=2.94, and T=4.36. (Bottom) From left to right, simulated skies for turbidities T=1.9, T=2.52, T=2.94, and T=4.36.

6. Evaluation

6.1 Turbidity estimation test

We tested our approach for turbidity estimation using static images of both simulated skies and real scenes. In the first case, we estimated turbidity 100 times taking Preetham sky models as input images. We used 100 sampling points for all of the estimations and provide the results in Table 1, where T_{mean} stands for the mean value of turbidity and T_σ stands for the corresponding standard deviation. Moreover, we tested the robustness of our method with respect of the sun direction estimation for the sky model of T=2 and showed the results and comparison with Zhao [4] in Table 2. In the second case, we estimated turbidity for omnidirectional captured images using 100 sampling points and 50 estimations per image, as illustrated in Fig. 6.

6.2 Aerial perspective model evaluation

Since we want to compare the synthesized aerial perspective obtained using our improved scattering model with the natural aerial perspective effect seen in real scenes, we evaluated our rendering model with real images taken at the same hour in different days.

6.2.1 Evaluation from a single real scene

We estimated the direct transmission and airlight constituents of a real image using our rendering model in Eq. (16). Figure 7 illustrates results obtained by our method and using Zhao's method [4] for different weather conditions. We can observe that our direct transmission is darker than Zhao's direct transmission, while our airlight component is brighter than Zhao's airlight. If we analyze the building in the red box (1729m from observer), in contrast to our method, Zhao's direct transmission tends to preserve airlight information (environment color). This feature in his method, which is more notorious for short distances, is wrong since direct transmission should not contain airlight information. On the other hand, if we observe the mountains surrounding Mount Fuji (50-100Km from observer) at T=1.9, opposed to our method, we notice that Zhao's airlight still keeps

mountains' contours. This aspect in his method contradicts McCartney's data [1], which says that the maximum discernible distance (meteorological range) for T=1.9 is around 20Km. In fact, these characteristics explain why Zhao's model makes a weaker aerial perspective effect (blurring and fading) than our model.

6.2.2 Evaluation from two real scenes

We analyzed two real scenes: one input image and one destination image. If we assume constant reflectance properties for objects under different weather conditions, $I_{0,c}/I_{\infty,c}$ in Eq. (16) should be constant for those objects in both input and destination images. Then our rendering model can be used to render aerial perspective using features of the input and destination images by

$$I_c(s) = I_c^{(1)}(s)\left[\frac{I_{\infty,c}^{(2)}}{I_{\infty,c}^{(1)}}\frac{\Gamma_c^{(2)}(s)}{\Gamma_c^{(1)}(s)}\right] + I_{\infty,c}^{(2)}\left[1 - \frac{\Gamma_c^{(2)}(s)}{\Gamma_c^{(1)}(s)}\right], \quad (18)$$

where I_c is the intensity value of a pixel with rendered aerial perspective. The upper indexes [1] and [2] correspond to features in Eq. (16) for the input and destination images respectively.

Figure 8 illustrates the synthesized aerial perspective by our method. We used the input image with T=1.9 in Fig. 7 as input image for all the evaluations since it provides more detailed color information than scenes with higher turbidities. As can be seen from the results, our method can generate color information that is consistent with the appearance of real images under different weather conditions.

7. Experimental results

All of the experiments were implemented in C++ and used a personal computer (OS: Windows 7; CPU: Corei7 2.93GHz; RAM: 16GB; GPU: nVIDIA GTX 550Ti 4049MB). We applied our rendering method to the Virtual Asukakyo (VA) project [10], which restores the ancient capital of Japan, Asukakyo, to its original status by using a MR system. The experiment took place near Asukakyo in a small hill named

Figure 7. Aerial perspective model evaluation from real single images. Comparison with Zhao's method. Top: T=1.9. Middle: T=2.94. Bottom: T=4.36.

Figure 8. Aerial perspective model evaluation from two images. Top: real images. Bottom: synthesized aerial perspective using our method.

Amakashioka (around 900m from Asukakyo). The captured image in Fig. 9 displays where Asukakyo lies. The height at the observer position was h_0=134m. The distance s of Asukakyo ruins from the observer was obtained from a depth map using Vinh *et al.* method [11].

As first part of the experiment, we rendered the VA with and without aerial perspective effect using our method and Zhao's method [4], as illustrated in Fig. 9. We applied our method and Zhao's method only to the virtual object.

In the second stage of our experiment, we modeled different weather conditions using Preetham sky models [2], as illustrated in Fig. 10. We obtained an image without aerial perspective effect using our method in Eq. (16) in reverse, that is, we calculated $I_{0,c}$. Then we applied our aerial perspective method and Zhao's method over the entire scene.

Table 1. Estimated turbidity using sky models as input images.

$T_{\text{sky model}}$	T_{mean}	T_σ
2.0	2.011791	0.004660
5.0	4.992700	0.055292
7.0	7.138090	0.062630
9.0	9.099154	0.089461

Table 2. Robustness of our turbidity estimation method.

Noise in sun direction	T_{mean}	T_σ	Our error	Error Zhao[4]
5 degree	2.018726	0.075164	0.93630%	3%
10 degree	2.062978	0.158684	3.14890%	5%
15 degree	2.102129	0.255967	5.10645%	9%

8. Discussion and Conclusion

In this paper, we have proposed an efficient turbidity-based method for rendering a virtual object with aerial perspective effect in MR. Our method estimates turbidity by matching the brightness distributions of a sky model and an omnidirectional captured image. In comparison with Zhao [4], our method is more robust to errors in sun position estimation and also does not depend on camera parameters.

We have also proposed an improved turbidity-based scattering model directed to MR applications. Our model benefits from McCartney's data [1] to classify scattering coefficient values via turbidity. Then we use this enhanced scattering model to provide a full-spectrum aerial perspective rendering model. Our rendering approach benefits from cameras' spectral sensitivity

provided in Zhao's work [4] to go from radiance light to RGB colors. In comparison with Zhao's aerial perspective model, our method is faster in the implementation and shows more realistic appearances of synthesized aerial perspective effect.

Although our rendered results applied to VA did not reach real time, we can handle this using a GPU. In fact, OpenGL provides an RGB-based fog simulator function [12] that can be used to emulate the aerial perspective effect. However, this fog function does not consider the full spectrum of light. Besides, this function needs the user to input an unknown fog's density value, which is impractical for MR applications.

Reference

1) E. McCartney. Optics of the atmosphere: scattering by molecules and particles. *John Wiley and Sons*, 1975.
2) A. Preetham, P. Shirley, and B. Smits. A practical analytic model for daylight. In *ACM Transactions on Graphics (SIGGRAPH)*, 1999.
3) S. Narasimhan and S. Nayar. Contrast restoration of weather degraded images. In *IEEE Transactions on Pattern Analysis and Machine Intelligence*, Vol. 25, No6, June 2003.
4) H. Zhao. Estimation of atmospheric turbidity from a sky image and its applications. *Ph.D dissertation*, The University of Tokyo, pages 13-30, 2012.
5) L. Rayleigh. On the scattering of light by small particles. In *Philosophical Magazine 41*, pages 447-454, 1871.
6) G. Mie. Beiträge zur Optik trüber Medien,speziell kolloidaler Metalllösungen. *Annalen der Physik 4*, 377–445, 1908.
7) R. Perez, R. Seals, and J. Michalsky. An all weather model for sky luminance distribution. *Solar Energy*, 1993.
8) S. Nayar and S. Narasimhan. Vision in bad weather. In *Proc. Seventh Int'l Conf. Computer Vision*, 1999.
9) R. Tan. Visibility in bad weather from a single image. In *CVPR'08*, pages 1-8, 2008.
10) Virtual Asukakyo Project:
http://www.cvl.iis.u-tokyo.ac.jp/research/virtual-asukakyo/
11) B. Vinh, T. Kakuta, R. Kawakami, T. Oishi, and K. Ikeuchi. Foreground and shadow occlusion handling for outdoor augmented reality. In *IEEE ISMAR*, pages. 109-118, 2010.
12) OpenGL fog. http://www.opengl.org/documentation

Figure 9. From top to bottom: real scene of Asukakyo (*T*=1.87), VA without aerial perspective, VA with our synthesized aerial perspective effect, VA with Zhao's synthesized aerial perspective effect.

Appendix
Weather condition via scattering coefficients
Table for spectrally weighted average wavelength (550 nm).

Table 3. Weather conditions via scattering coefficients in Km^{-1} [1]

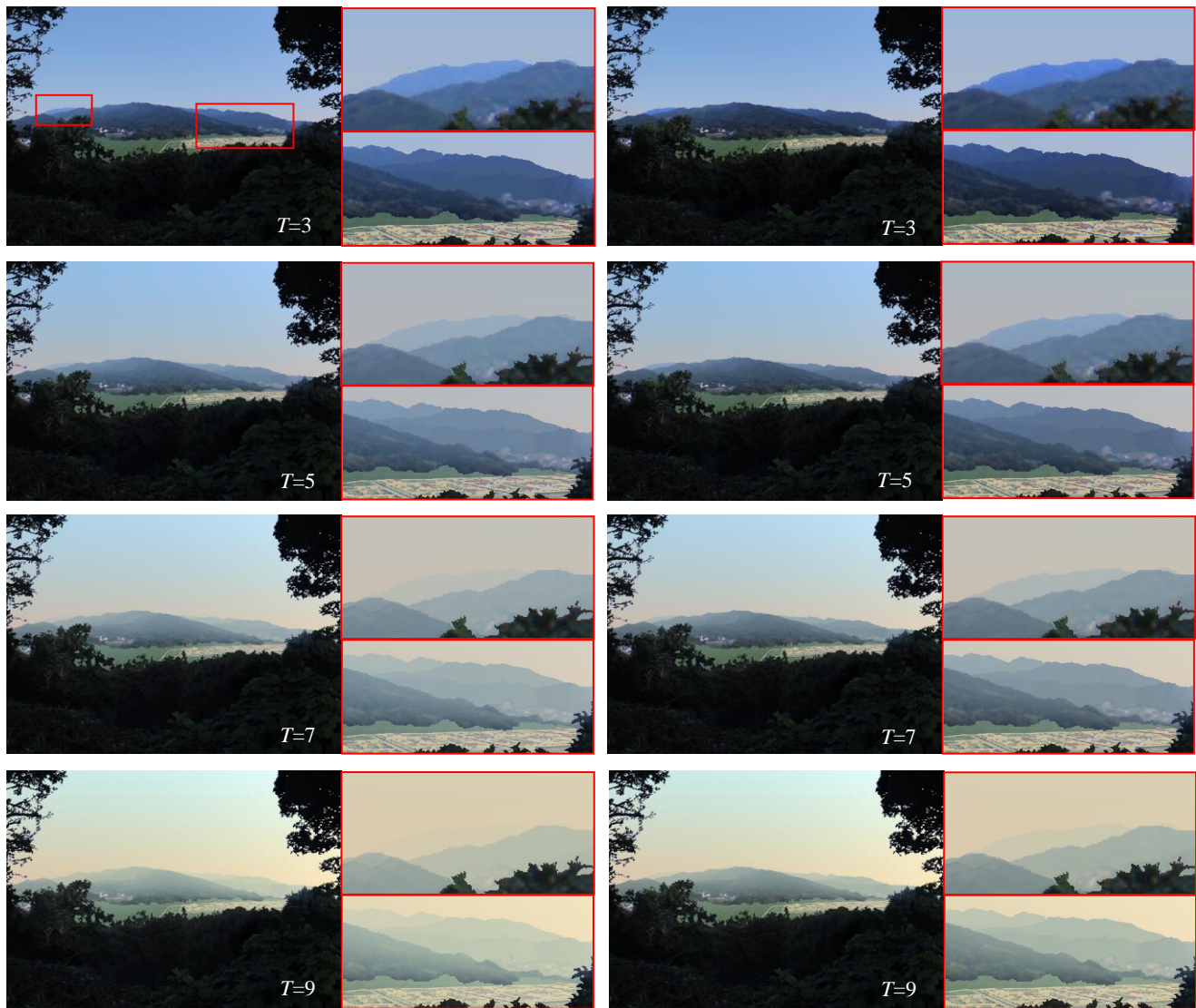| Condition	β_M	Min β_R	Max β_R
Pure air	0.0141	0	0
Exceptionally clear	0.0141	0.0639	0.0639
Very clear	0.0141	0.0639	0.1819
Clear	0.0141	0.1819	0.3769
Light haze	0.0141	0.3769	0.9399
Haze	0.0141	0.9399	1.9459
Fog	0.0141	1.9459	>78

Figure 10. Aerial perspective effect applied to entire scene except the sky. Left column: rendered with our method. Right column: rendered with Zhao's method.